JCTC Journal of Chemical Theory and Computation

Article

pubs.acs.org/JCTC

Convergence of QM/MM and Cluster Models for the Spectroscopic Properties of the Oxygen-Evolving Complex in Photosystem II

Marius Retegan, Frank Neese, and Dimitrios A. Pantazis*

Max Planck Institute for Chemical Energy Conversion, Stiftstr. 34-38, 45470 Mülheim an der Ruhr, Germany

Supporting Information

ABSTRACT: The latest crystal structure of photosystem II at 1.9 Å resolution, which resolves the topology of the Mn_4CaO_5 oxygen evolving complex (OEC) at atomistic detail, enables a better correlation between structural features and spectroscopic properties than ever before. Building on the refined crystallographic model of the OEC and the protein, we present combined quantum mechanical/molecular mechanical (QM/MM) studies of the spectroscopic properties of the natural catalyst embedded in the protein matrix. Focusing on the S_2 state of the catalytic cycle, we examine the convergence of not only structural parameters but also of the intracluster magnetic interactions in terms of exchange coupling constants and of experimentally relevant ^{55}Mn, ^{17}O, and ^{14}N hyperfine coupling constants with respect to QM/MM partitioning using five QM regions of increasing size. This enables us to assess the performance of the method and to probe second sphere effects by identifying amino acid residues that principally affect the spectroscopic properties of the OEC. Comparison between QM-only and QM/MM treatments reveals that whereas QM/MM models converge quickly to stable values, the QM cluster models need to incorporate significantly larger parts of the second coordination sphere and surrounding water molecules to achieve convergence for certain properties. This is mainly due to the sensitivity of the QM-only models to fluctuations in the hydrogen bonding network and ligand acidity. Additionally, a hydrogen bond that is typically omitted in QM-only treatments is shown to determine the hyperfine coupling tensor of the unique Mn(III) ion by regulating the rotation plane of the ligated D1-His332 imidazole ring, the only N-donor ligand of the OEC.

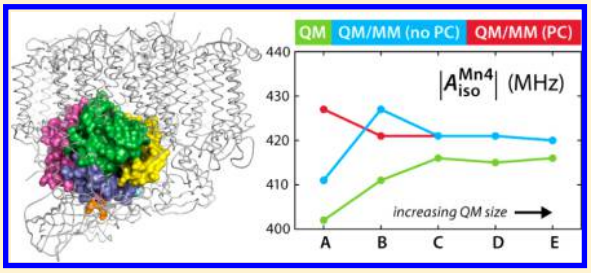

1. INTRODUCTION

The ability to reliably describe the electronic structure of a molecular model from quantum chemical calculations and to predict its ensuing magnetic and spectroscopic properties with a level of confidence that allows comparisons with experimental results has become instrumental in addressing many persisting questions in bioinorganic chemistry. Studies on complex open-shell transition metal species in the active sites of metalloproteins, such as the manganese−calcium cluster of photosystem II (PSII),[1−7] best demonstrate not only the challenges in applying high-level theoretical methods[8,9] but also the rewards of successfully combining experimental and computational spectroscopy.[7]

PSII, the photosynthetic enzyme that uses light to split water, is a prominent example of a highly complicated bioinorganic system where several techniques and approaches are brought to bear on the problem of establishing the structure and operating principles of its catalytic site, the oxygen evolving complex (OEC). The OEC consists of an inorganic Mn_4CaO_5 cluster embedded in a functionally important and evolutionarily conserved protein matrix (Figure 1). It operates by storing up to four oxidizing equivalents to catalyze the splitting of two water molecules and evolve dioxygen. The singular importance of this reaction has fueled extensive efforts to clarify the structure and function of the OEC as the basis of natural photosynthesis and as a potential blueprint for artificial solar-fuel systems.[10−12]

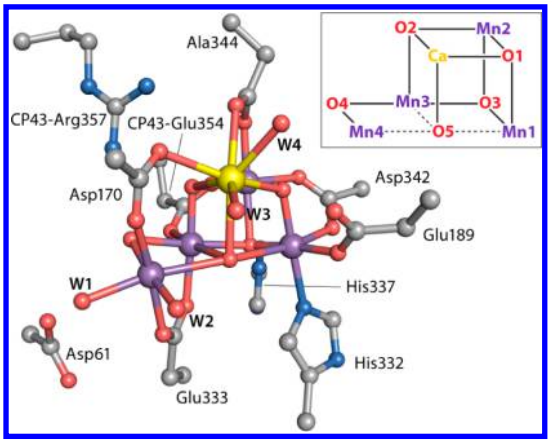

Figure 1. The Mn_4CaO_5 cluster of the OEC and its immediate protein environment as determined in the 1.9 Å X-ray model of PSII by Umena et al.[15] The labeling scheme for the Mn_4CaO_5 core atoms shown in the inset is followed throughout this paper.

Received: June 7, 2013
Published: July 12, 2013

The challenge of describing the electronic structure and calculating the observable properties of a cluster composed of magnetically interacting open-shell transition metal ions is compounded by the size of the computational models, which typically for the OEC contain up to a few hundred atoms. There are both lower and upper limits to the size of the models that can be treated. For example, our present knowledge of the catalyst suggests that a model must be large enough to include a number of water molecules and second sphere residues that form a complex hydrogen bonding network around the Mn_4O_5Ca core. On the other hand, upper limits are imposed by practical restrictions. For example, charged amino acid residues beyond the first coordination sphere may affect the predicted magnetic and spectroscopic properties of a model, but most of them cannot be accommodated even in the biggest quantum mechanical (QM) OEC models currently employed. A way out of this conundrum is the treatment of the nonimmediate surrounding of the OEC with molecular mechanics (MM) in a combined QM/MM approach.[13,14] Besides the inclusion of long-range structural and electrostatic effects, this can permit a controlled reduction of the QM size without sacrificing the demonstrated accuracy of large but expensive QM-only approaches for spectroscopic parameters.

QM/MM studies on the OEC were first performed by Batista and co-workers, who proposed not only structural models, initially derived from modifications of a 3.5 Å resolution X-ray diffraction (XRD) structure[16] but also possible reaction steps for the complete water oxidation cycle.[17−23] Siegbahn, however, suggested that these models do not correspond to stable minima in QM-only cluster calculations.[24] Moreover, following the 1.9 Å resolution XRD structure of PSII,[15] the models were confirmed to be inconsistent with current information on the stoichiometry of the manganese−calcium core (four oxo bridges instead of five in the crystal structure), the position of a chloride ligand (assumed to be directly bonded to Ca^{2+} instead of being more than 9 Å away, at the opposite side of the Mn_4CaO_5 cluster[15,25,26]), and the metal−protein connectivity (nature and coordination mode of first sphere residues, particularly Asp170). In view of these discrepancies, a new model that is based on the more recent structural information was proposed for the S_1 state,[27] whereas the other states of the proposed catalytic cycle[20] have not yet been updated. Siegbahn has used instead QM-only cluster models to refine the structure of the OEC,[28] applying backbone constraints to simulate the effect of the protein structure[29] and using the lowest possible energy barriers for O−O bond formation as the main guiding principle.[30−33] This approach led to the first computational model that was broadly consistent both with a range of experimental spectroscopic parameters[34−36] and with the latest XRD structure of PSII.[15]

The approach followed by our group has focused on the magnetism and spectroscopy of OEC models,[34,37,38] with the aim of correlating structural features with spectroscopic properties.[35,36] This line of attack employs theoretical methods for the prediction of experimental observables[39] that relate to results of electron paramagnetic resonance (EPR) and pulse magnetic resonance techniques. As in most other work that deals with the electronic structure of the OEC,[40−62] these spectroscopy-oriented studies have followed the QM-only approach and have gradually improved in completeness over the years by increasing the size of the model up to almost 300 atoms.[38] Detailed insights into the spectroscopic features of the OEC have been obtained this way,[7,35−38,63] but the computational cost of the increased accuracy becomes untenable if extensive exploration of the conformational space or adequate sampling of reaction pathways are desired. Hence, it would be ideal if the most appealing features of all the above-mentioned approaches are merged into a single unified treatment.

In the present paper, we attempt to develop a protocol by which (a) the best possible geometry of the inorganic Mn_4CaO_5 core of the OEC is employed, as revealed by the latest X-ray structure of PSII[15] and refined according to spectroscopic information,[38] (b) the OEC is embedded in an extended protein matrix using a QM/MM approach, and (c) the quantum chemical methods that have enabled successful calculations of spectroscopic observables in QM-only models[34,39,64] are extended, adapted, and applied within the QM/MM scheme. The goals of this study are (a) to verify the optimal QM/MM approach in a rigorous way, which consists of studying the convergence of magnetic and spectroscopic properties with respect to the QM/MM partitioning, and (b) to examine the influence of residues beyond the first coordination sphere on properties of interest. These effects may be purely electrostatic or may propagate through extensive H-bonding networks, but may in either case be absent from QM-only models. This is precisely what is demonstrated here for the charged residues Asp61 (all residues without chain identifiers refer to the D1 polypeptide), CP43-Arg357, and His337, which either interact with the inorganic Mn_4CaO_5 core via hydrogen bonding to its oxo-bridges (CP43-Arg357 and His337), or dictate the coordination and protonation state of manganese-bound water ligands (Asp61). The rotation of the Mn(III)-coordinating His332 residue, which depends on directional interactions with a protein region beyond that included in any plausible QM-only model, is shown to have a significant influence on the predicted spectroscopic signature of the OEC in the form of ^{55}Mn hyperfine coupling constants.

2. METHODOLOGY

2.1. Initial Coordinates, Force Field, and Model Preparation. The starting point for the present model was the 1.9 Å resolution XRD structure by Umena et al.[15] The size of the QM/MM model was restricted to a quasi-spherical region around the Mn_4CaO_5 cluster, comprising all amino acid residues and water molecules with at least one atom within 20 Å from any atom of the Mn_4CaO_5 cluster (Figure 2). Where possible, we ensured that the model has continuous loops by adding the missing amino acids.

Development of bonding force field parameters for the Mn_4CaO_5 cluster was beyond the scope of the present study, so in all the classical simulations, the position of heavy atoms from the OEC core, the coordinating residues, Asp61, His337, and Arg357, were harmonically restrained to their crystallographic coordinates with a force constant of 100 kJ mol^{-1} Å^{-2}. The OPLS-AA force field[65] was used for the protein and the ions and the TIP3P model[66] for the water molecules. For the Mn_4CaO_5 cluster, partial charges were assigned as follows: Ca = +2.0, Mn1 = +1.5, Mn2 and Mn3 = +2.0, and O1−O5 = −0.5, while Lennard−Jones parameters were adapted from the OPLS-AA force field. The protonation states of residues were based on the PROPKA 3.0[67] results and were verified by visual inspection. The system was solvated in a pre-equilibrated water box of dimensions 72 × 73 × 75 Å and was neutralized by adding three chloride ions. The final system included 39 648 atoms.

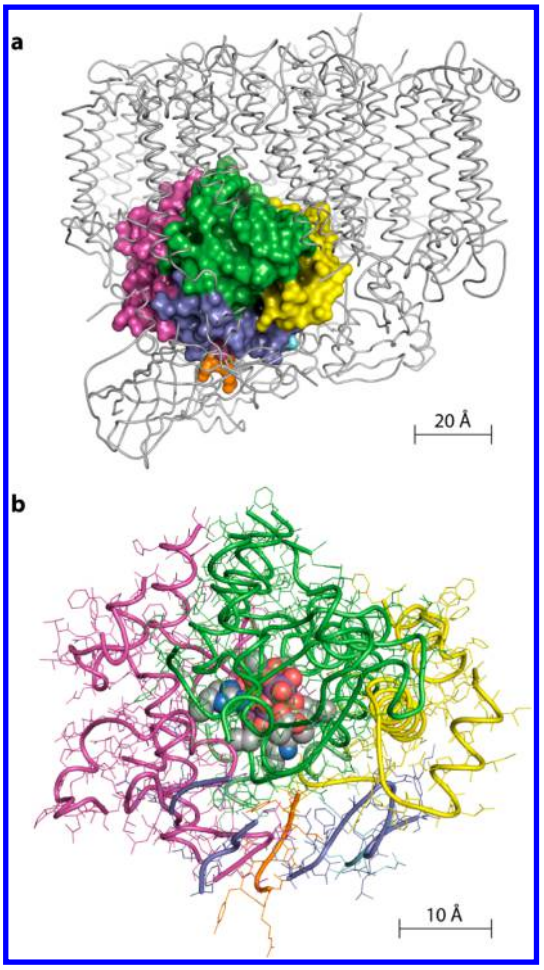

Figure 2. (a) The part of the protein considered explicitly in the present study. The QM/MM region (in color) is shown within a PSII monomer from the XRD structure of Umena et al.[15] (b) The QM/MM model (depicted unsolvated), with QM atoms represented as spheres.

The positions of hydrogen atoms were relaxed by 2000 steps of energy minimization with the L-BFGS algorithm. The solvent was subsequently equilibrated by performing 100 ps of NVT molecular dynamics simulations. Afterward, the system was annealed from 50 to 300 K over the course of 100 ps. During these simulations, the heavy atoms were harmonically restrained to the crystallographic positions with a force constant of 10 kJ mol^{-1} $Å^{-2}$. The production simulation consisted of 300 ps of NPT (T = 300 K and P = 1 bar) molecular dynamics simulation. The temperature and pressure were controlled by a Langevin thermostat and Parrinello−Rahman barostat with the coupling time constants 2.0 and 0.5 ps, respectively. The long-range electrostatic interactions were treated with the particle mesh Ewald (PME) summation beyond a cutoff of 12 Å, while the Lennard-Jones interactions were smoothly switched off from 10 Å to 12 Å. The neighbors list was updated every five steps. An integration time step of 1.0 fs has been used. The simulations were performed with the GROMACS 4.5.5 package.[68] In order to avoid protein denaturation at the periphery, the harmonic restraints on the heavy atoms outside the 15 Å region around the cluster were retained during the production phase. The last structure of the equilibration phase was used as the starting point for all the geometry optimizations and subsequent calculations of magnetic properties.

2.2. QM Region Models. Five QM regions of increasing size were evaluated in order to investigate the point of convergence for each property of interest (Figure 3). The smallest QM region **A** consisted of 92 QM atoms and included the first-sphere ligated side chains of Asp170, Glu189, His332, Glu333, Asp342, CP43-Glu354, the entire Ala344 residue, and the carbon and oxygen atoms from the Leu343 backbone, as well as the directly coordinating water molecules HOH1000 (W1), HOH999 (W2), HOH541 (W3), and HOH540 (W4). The four coordinating waters are taken as neutral, terminal H_2O ligands, and the five core oxygen atoms are considered to be unprotonated oxo bridges. Considerations of different protonation patterns are of no relevance in the present work.[37] The larger QM region **B** (131 atoms) expanded upon region **A** by including the side chains of Asp61, His337, and CP43-Arg357, all of which interact with the OEC cluster via hydrogen bonding. Region **C** (155 atoms) includes region **B** and eight additional water molecules HOH358, HOH428, HOH442, HOH446, HOH538, HOH539, HOH542, and HOH923, all of which form an extended hydrogen bonding network around the inorganic core of the OEC. Region **D** (183 atoms) expanded region **C** by including the side chains of the redox-active Tyr161 (Y_Z) and its hydrogen-bonded partner His190. Finally, the largest QM region employed (**E**, 225 atoms) included in addition to region **D** the proximal catalytically important chloride ion (Cl679) and its immediate environment, i.e. the side chains of Asn181 and D2-Lys317, the D2-HOH544 water molecule, the backbone of His332 and Glu333, and the carbon and oxygen atoms from the backbone of the Met331 residue.

2.3. Hybrid QM/MM Simulations. The QM/MM calculations were carried out with an electrostatic embedding scheme. In order to reduce the number of integrals involving point charges, water molecules 2.5 Å away from the protein or 20 Å away from Mn_4CaO_5 cluster were removed. The final QM/MM system consisted of 8658 atoms. The MM part was treated at two levels during the QM/MM optimizations. All MM atoms that were within 10 Å of the Mn_4CaO_5 cluster were fully allowed to relax and adapt to the QM geometry changes, while all MM atoms beyond this radius were constrained to their initial positions in order to maintain the observed secondary structure of the protein. For the geometry optimizations, the QM region was described with the BP86 functional[69,70] assuming a total high-spin state (ferromagnetic alignment of the individual Mn spins) and using the zeroth-order regular approximation (ZORA) Hamiltonian[71−74] to account for scalar relativistic effects. The ZORA-recontracted[75] def2-TZVP(-f) basis sets were used for all atoms, except for H and C, for which the basis set was reduced to the ZORA def2-SVP.[76] The resolution of identity approximation with appropriate auxiliary basis sets[77] was used to speed up the calculations. The van der Waals correction terms by Grimme (DFT-D3) were included to account for dispersion effects within the QM part during geometry optimizations.[78] The MM region was described with the OPLS all-atom force field. When possible we ensured that the border between the QM and MM regions was placed on the C_α−C_β bond. The free valences were capped with hydrogen link atoms, and the charge redistribution scheme was applied to avoid overpolarization effects.[79] The full MM and QM/MM nonbonded interactions were calculated. The initial geometry was optimized by performing 100 steps of

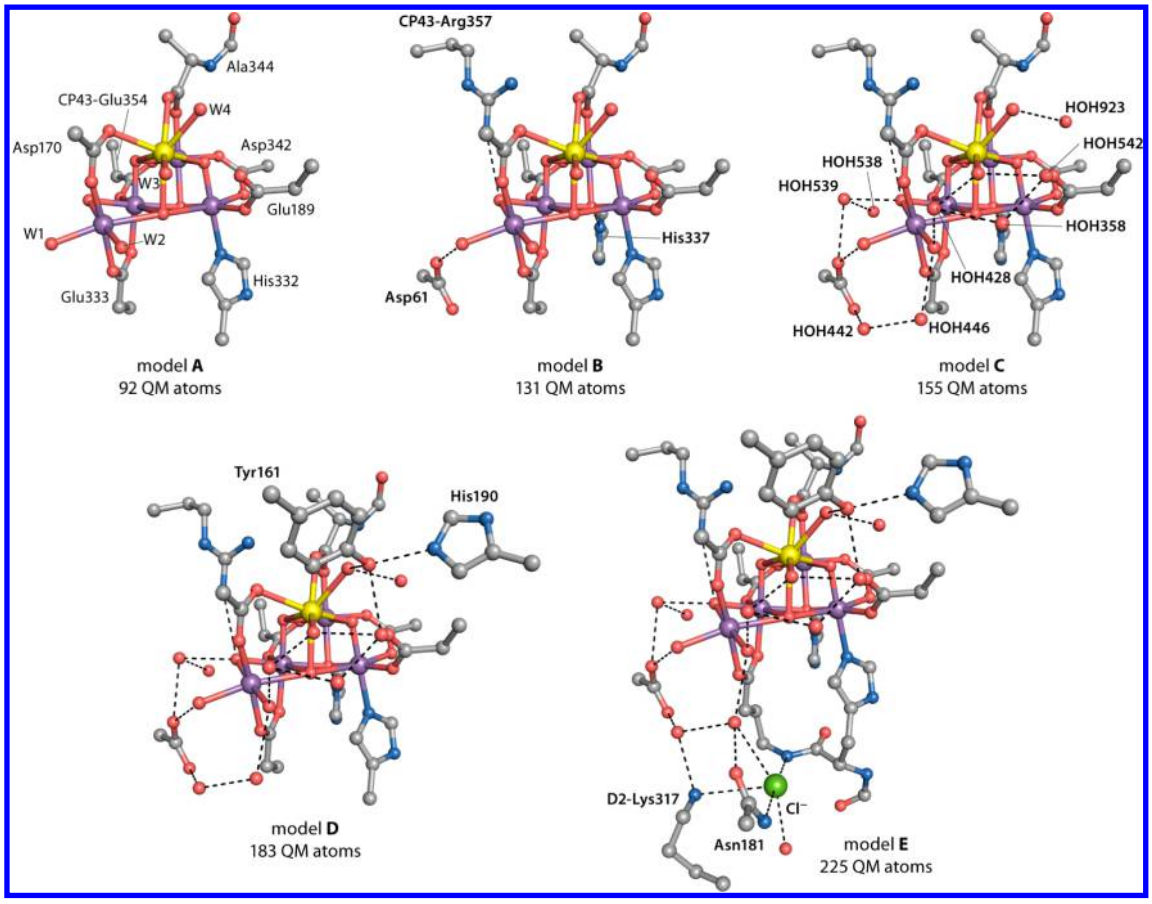

Figure 3. The five QM regions employed in this study, indicating the additions made at each enlargement step and the total number of QM atoms. Hydrogen atoms are omitted for clarity.

conjugate gradient followed by L-BFGS minimization until the root-mean-square gradient was below 10^{-3} kJ mol^{-1} Å^{-2}. All QM/MM computations were performed with the pDynamo 1.7.2 library[80] that provides the MM description of the system and an interface to the ORCA 2.9 program[81] for the QM region.

2.4. QM-Only Simulations. The same theoretical level employed to describe the QM region in the QM/MM setup was used for the QM-only calculation. The approximate effect of the missing MM atoms was modeled by constraining the beta carbons and the bound hydrogen atoms, and by employing the conductor-like screening model (COSMO) with a dielectric constant of 4.[82]

2.5. Calculations of Magnetic and Spectroscopic Properties. Broken symmetry DFT calculations using all possible single-flip and double-flip spin-alignment combinations for the extraction of pairwise exchange coupling constants with singular value decomposition, diagonalization of the Heisenberg−Dirac−van Vleck (HDvV) Hamiltonian to obtain the full spectrum of energy levels, and calculation of hyperfine tensors follow protocols developed and discussed in previous papers that employed QM-only models for the OEC and related manganese systems.[34,37−39,64,83−86] The hybrid meta-GGA TPSSh functional[87] with the ZORA scalar relativistic Hamiltonian and the ZORA-recontracted def2-TZVP(-f) basis sets for all elements were used for the broken-symmetry single point calculations and for all magnetic and spectroscopic properties. The isotropic hyperfine coupling constant for nucleus K obtained from a broken-symmetry DFT calculation ($A^{(K)}_{iso,BS}$) must be spin-projected to a value $A^{(K)}_{iso}$ that can be meaningfully compared with experimental results.[39] The transformation is defined as

$$A^{(K)}_{iso} = \pm A^{(K)}_{iso,BS}\left(\frac{\langle S_z\rangle_{BS}}{S_A}\right)\left(\frac{\langle S_z^{(A)}\rangle}{S_T}\right)$$

where S_T is the total spin and $\langle S_z\rangle_{BS}$ is the total M_S of the broken-symmetry wave function. The on-site spin expectation value $\langle S_z^{(A)}\rangle$ is obtained as

$$\langle S_z^{(A)}\rangle = \sum_{S_A M_{S_A} \ldots S_N M_{S_N}} |C_I^{\,S_A M_{S_A} \ldots S_N M_{S_N}}|^2 M_{S_A}$$

where coefficient C_I represents the weight of the basis state $I = |S_A M_{S_A} \ldots S_N M_{S_N}\rangle$ in the ground-state eigenfunction of the HDvV Hamiltonian $|S_A S_B \ldots S_N, S M_S\rangle$ with $S = M_S$.[39] To facilitate comparisons with experimental data, the spin-projected values can be scaled by a common factor in order to counteract the systematic underestimation of core spin polarization by DFT. This scaling factor is 1.78 for the present methods (density functional, treatment of relativity, and basis sets), based on calibration with a set of Mn(III/IV) mixed-valence dimers taken from ref 64 (complexes 2−13 of that work).

Note that spin-projected (and scaled) hyperfine coupling constants, which are reported in the Supporting Information, are not directly relevant for the purposes of this work, as the "raw" hyperfine values are sufficient to study the convergence behavior of each approach. It should also be noted that a proper

Table 1. Selected Interatomic Distances (Å) for the Geometry-Optimized Models, Compared with Average Distances from EXAFS

	Mn1−O5	Mn4−O5	Mn1−Mn2	Mn2−Mn3	Mn3−Mn4	Mn1−Mn3	Mn1,2,3,4−Ca
$\mathbf{A}_{QM/MM}$	2.98	1.83	2.79	2.77	2.69	3.27	3.58, 3.46, 3.77, 4.09
$\mathbf{B}_{QM/MM}$	2.94	1.85	2.81	2.78	2.71	3.28	3.55, 3.50, 3.81, 4.09
$\mathbf{C}_{QM/MM}$	2.91	1.85	2.81	2.78	2.72	3.27	3.56, 3.44, 3.71, 3.99
$\mathbf{D}_{QM/MM}$	2.87	1.85	2.81	2.77	2.71	3.26	3.57, 3.48, 3.79, 4.04
$\mathbf{E}_{QM/MM}$	2.91	1.85	2.81	2.77	2.71	3.27	3.57, 3.46, 3.75, 4.02
EXAFS				2.7, 2.8 (2:1)		3.3	3.4, 3.9 (2:2 or 3:1)

comparison with experimental data would in principle require ensemble averaging, since for such large systems many conformers can exist that lie close in energy and may differ slightly in their spectroscopic properties. This would be a common requirement for both QM and QM/MM approaches and would not affect the convergence behavior studied in this work. However, it is an issue that has not been sufficiently addressed in studies of PSII and may need more serious consideration in the future, especially given the emerging view of inherent structural flexibility in the OEC.[38]

3. RESULTS AND DISCUSSION

The five models QM/MM ($\mathbf{A}_{QM/MM}$−$\mathbf{E}_{QM/MM}$) and their corresponding QM-only models ($\mathbf{A}_{QM}$−$\mathbf{E}_{QM}$) define a progression of chemically sensible QM regions of increasing size and complexity, without exclusively following a simplistic distance-based criterion. In the following, we examine how the geometry of the cluster, its electronic structure, the magnetic interactions between the Mn ions, and all properties derived from those converge with respect to the size of the QM region.

It is emphasized from the outset that all models have the same III−IV−IV−IV distribution of oxidation states among the Mn ions; that is, the Mn1 center is always the unique Mn(III) ion of the cluster. Additionally, the manganese spin populations are consistent for all QM/MM and cluster models considered in this work and very close to the formal number of unpaired spins for Mn ions with local high-spin electronic configurations forming predominantly ionic bonds (∼3.9 for Mn1 and ∼2.9 for the remaining Mn(IV) centers). This is typical of high-valent manganese systems.

3.1. Structural Parameters. We start by analyzing the structural data obtained with QM/MM models of increasing QM size. Selected distances are summarized in Table 1. The geometry of the cluster is not critically influenced by inclusion of additional residues in the QM region. Model **B** can be considered converged, but already with the smallest reasonable model **A** the calculated Mn−O bond lengths and Mn−Mn and Mn−Ca distances are in good agreement with the larger models. The largest deviation with these models was found for the Mn1−O5 distance. This is presumably linked to the higher flexibility of the terminal Mn4—the "dangling" manganese—compared with the environment of the remaining manganese ions and the increased flexibility of O5 compared to the other oxo bridges.[38] Thus, in terms of variability upon geometry optimizations, this particular topology of the OEC core behaves as a hinge under different settings, with Mn3 defining the joint.

All the models are in good agreement with the EXAFS distances, supporting the assignment of the Mn1−Mn3 distance as the "long" distance (∼3.3 Å) in the measured spectra, since all other Mn−Mn distances longer than the "short" EXAFS distances (∼2.7−2.8 Å) exceed 4 Å. This agrees with experimental assignments.[88] Regarding the Mn−Ca distances, we find a larger deviation within the calculated values, but they are nevertheless consistent with experimental data[89] and lean toward a 2:2 model with Mn3−Ca and Mn4−Ca as the longer distances.

At this point, it would be instructive to compare these structural parameters with the corresponding ones obtained by optimizing the QM-only cluster models, in which the protein environment is modeled by an implicit solvent with a small dielectric constant ($\varepsilon = 4$). The QM-only results are reported in Table S1. Overall, the structural parameters are similar with the ones obtained from QM/MM, but only starting from model $\mathbf{C}_{QM}$ can they be considered converged. As noted before, the largest deviation is found for the Mn1−O5 distance, and it is more pronounced for the small QM-only models. The smaller value calculated for model $\mathbf{A}_{QM}$ is most probably due to either the 67° rotation of the imidazole ring of His332 with respect to the manganese core or the absence of Asp61 which is hydrogen-bonded to W1. The different alignment of His332 with respect to the Mn_4CaO_5 cluster is traced to a missing hydrogen bond between the π-N (Nδ) of the imidazole ring and the oxygen atom from the backbone carbonyl group of Glu329. Similarly pronounced are the changes in Mn−Ca distances: with the exception of the Mn1−Ca distance, they are all shorter by approximately 0.2 Å in the $\mathbf{A}_{QM}$ compared to the $\mathbf{A}_{QM/MM}$ model. The most probable cause for this is the formation of a hydrogen bond between W2 and W3 during the QM-only geometry optimization. This results in an apparent compression of the inorganic core that is not observed in either the QM/MM models or the larger QM-only models. In those, as in the XRD structure, an alternative hydrogen bonding network is established, in which W3 is—correctly—hydrogen-bonded to Tyr161. It is emphasized that this arrangement of hydrogen bonds is present even in the smallest QM/MM model $\mathbf{A}_{QM/MM}$, which comprises the same number of QM atoms as the small QM-only model $\mathbf{A}_{QM}$. This highlights a potential drawback of using small QM-only cluster models: structural artifacts during their optimization, which may arise even due to the absence of a few hydrogen-bond directing groups, can induce modifications of the magnetic properties, as will be further elaborated in the following.

3.2. Exchange Coupling Constants. The exchange coupling constants for all the QM/MM models are collected in Table 2. The magnetic coupling pattern and the magnitude of the individual exchange couplings is consistent with previous studies.[35−38] Higher values are obtained for three of the six couplings, with an antiferromagnetic interaction for the Mn1−Mn2 and Mn3−Mn4 pairs and a ferromagnetic interaction for the Mn2−Mn3 pair. The exchange coupling constants are considerably smaller and are close to zero for pairs of ions for which the interaction is not directly mediated by oxo bridges, e.g. Mn2−Mn4, or for ions that are coupled by only one such bridge, e.g. Mn1−Mn3. A somewhat larger value is obtained for

Table 2. Computed Exchange Coupling Constants J_{ij} (cm^{-1}) and Energetic Separation between the Ground and the First Excited State (cm^{-1})

	J_{12}	J_{13}	J_{14}	J_{23}	J_{24}	J_{34}	ΔE_{ES-GS}
$\mathbf{A}_{QM/MM}$	−20	1	5	19	2	−15	27.2
$\mathbf{B}_{QM/MM}$	−19	3	5	21	2	−17	26.3
$\mathbf{C}_{QM/MM}$	−20	3	6	21	2	−17	27.1
$\mathbf{D}_{QM/MM}$	−20	3	6	21	2	−17	26.4
$\mathbf{E}_{QM/MM}$	−20	3	6	21	2	−17	26.8

the coupling between Mn1−Mn4. One should keep in mind that while in the case of dimers these magnetic couplings can be rationalized to some extent on the basis of pairwise magnetic orbital overlap between the metal centers and the bridging atoms,[85] the present case cannot be as easily decomposed into a simplified view of interacting pairs.[86] An example of an alternative approach is the substitution of paramagnetic centers by diamagnetic ions of the same formal charge and similar ionic radius (e.g., Ge^{4+} for Mn^{4+}) in order to reduce again the problem into distinct magnetic pairs. However, as recently demonstrated for the case of Mn_3CaO_4 cubanes, even though this approach may provide visually informative results in terms of corresponding orbitals it does not necessarily recover the complete description of the system.[86]

A similar distribution of exchange coupling constants was observed in the case of the QM-only models, with a larger value obtained for centers that interact through oxo bridges (Table S2). The convergence of the exchange coupling constants follows the trend observed for the structural parameters, with larger variations observed for the smaller models. Nevertheless, even for the larger QM-only models, the convergence with increasing size is not as smooth as that observed for the QM/MM models. The origins of these differences for the larger QM-only models are not immediately obvious, but they can be tentatively assigned to small modifications in the environment of the inorganic core as a result of adding another outer layer of atoms. While these additional atoms represent the interaction partners for the "inner" atoms of the smaller QM-only model, they are in turn missing some of their "outer" interaction partners, a situation that can maintain or even introduce new sources of structural artifacts during optimization, thus delaying geometric convergence.

According to the eigenvalues of the HDvV Hamiltonian obtained for each individual structure, all models have a ground state with total spin $S_t = 1/2$. The calculated energy gaps between the ground state and the first $S_t = 3/2$ excited state are all similar for the QM/MM models, within the narrow range 26−27 cm^{-1}. Compared with all other QM or QM/MM models, a small energy gap of 15 cm^{-1} is obtained for $\mathbf{A}_{QM}$ owing to significant differences in the computed exchange coupling constants. According to our simulations and to previous experimental work,[35,36] the magnitude of J_{34}, the exchange coupling constant that corresponds to the bis-μ-oxo bridged Mn(III,IV) subunit of the OEC in the S_2 state, is a critical regulator of the spin ladder spacing. Thus, the reduction in the magnitude of J_{34} by more than 100% in $\mathbf{A}_{QM}$ compared with the value of average −22 cm^{-1} obtained for the larger QM-only models appears to be the origin of the different description of the energy level structure.

3.3. Isotropic Hyperfine Coupling Constants. From a theoretical point of view, the hyperfine coupling constants (HFCs) can be computed by spin-projecting the raw values obtained from the lowest energy broken-symmetry wave function. The steps involved in the determination of the spin expectation value of the S_z operator have been described previously,[39] and the introduction of the spin Hamiltonian matrix for the present case is parametrized in a first approximation by the exchange coupling constants. Since both the raw hyperfine values and the exchange couplings are affected by the electronic structure, it would be difficult to discern whether the differences between the models are due to perturbation of the exchange pathways or to the intrinsic hyperfine values themselves. Hence, we limit our discussion here to the raw hyperfine coupling constants, which are summarized in Table 3. Projected values (see eq 1) are reported along with the local spin expectation values in Table S3 of the Supporting Information.

Table 3. Calculated Values for the Unscaled and Unprojected ^{55}Mn Isotropic Hyperfine Coupling Constants (MHz) of QM/MM Models

	Mn1	Mn2	Mn3	Mn4
$\mathbf{A}_{QM/MM}$	−259	366	362	−427
$\mathbf{B}_{QM/MM}$	−254	364	358	−421
$\mathbf{C}_{QM/MM}$	−252	365	355	−421
$\mathbf{D}_{QM/MM}$	−253	366	355	−421
$\mathbf{E}_{QM/MM}$	−255	366	357	−420

Trends noted in the case of the geometrical parameters and exchange coupling constants also apply to the present case: increasing the QM region in the QM/MM model has limited influence on the calculated properties. Interestingly, for $\mathbf{A}_{QM}$ (see Table S4 for QM-only results) the isotropic hyperfine coupling constants differ significantly, especially for the two "terminal" OEC ions Mn1 and Mn4, which are in the oxidation states of III and IV, respectively. The absolute A_{iso} value of Mn1 is approximately 100 MHz larger for $\mathbf{A}_{QM}$ compared with the QM/MM models. Whereas by increasing the size of the QM-only models the HFC of Mn4 converges to the value obtained with the QM/MM models, even with the largest model—model **E**—the HFC of Mn1 is still approximately 50 MHz larger compared to the QM/MM model. These changes can be related to structural modifications of the cluster itself—the Mn1−O5 distance is reduced by approximately 0.2 Å in the QM-only model—but also to changes in orientation of the coordinating amino acid residues, as noted previously for His332. As practiced in previous work, such artifacts in QM-only calculations can be avoided by a costly "brute force" increase in the size of the model, but the present results suggest that this increase is beyond what is adequate in a QM/MM calculation.

In addition to ^{55}Mn nuclei, we have also investigated the convergence behavior of the isotropic ^{17}O HFCs of the O5, W1, and W2—all coordinated to Mn4—and ^{14}N HFC of the nitrogen atom of His332, which is directly coordinated to Mn1. These ligands serve as important spectroscopic reporters of the electronic structure of the Mn_4CaO_5 cluster in its various states and as it is perturbed by the binding of substrate analogs.[36,63] For the QM/MM models, the calculated isotropic hyperfine coupling constants show only small differences with increasing QM size, the largest deviations being observed for model $\mathbf{A}_{QM/MM}$ (Table 4). The ^{17}O HFCs of the Mn4-bound waters are the parameters that are most affected; however, with the

dx.doi.org/10.1021/ct400477j | J. Chem. Theory Comput. 2013, 9, 3832−3842

Table 4. Calculated Values for the Unscaled and Unprojected ^{17}O and ^{14}N Isotropic Hyperfine Coupling Constants (MHz) of QM/MM Models

	O5	W1	W2	Nε (His332)
$A_{QM/MM}$	−15.3	−3.7	2.8	−12.6
$B_{QM/MM}$	−17.7	−6.1	0.6	−12.4
$C_{QM/MM}$	−18.0	−5.1	0.6	−12.2
$D_{QM/MM}$	−19.6	−5.3	0.8	−12.3
$E_{QM/MM}$	−18.3	−5.2	0.4	−12.2

inclusion of the amino acids in the second coordination sphere all values quickly converge.

3.4. Convergence of Structural and Spectroscopic Properties. Overall, from the results of the calculations presented above, it can be concluded that the QM/MM calculations converge quickly and smoothly with respect to the size of the QM region. Inclusion of residues and water molecules that are hydrogen-bonded to the inorganic core of the OEC is necessary, but extension of the QM region beyond this basic model does not translate to significant changes. Thus, even QM/MM model **B** is sufficient to obtain converged structural parameters and exchange coupling constants. Calculations of hyperfine coupling constants are somewhat more sensitive to the size of the QM region; however, the results are converged for practical purposes already for models like **B** and **C**, which, with 131 and 152 QM atoms, respectively, are still only half the size of the largest QM-only models employed in recent computational studies.

For the QM-only models, the structural parameters of the inorganic core can be considered already converged using model $\mathbf{C}_{QM}$. While similar trends are observed for the spectroscopic properties, the convergence is less smooth as can be seen for the ground state−first excited state energy gap, the exchange coupling constant, and the isotropic hyperfine coupling constants of the manganese ions (Figure 4). These differences, which are present even for the two largest QM-only models, can be associated with geometrical changes resulting from increasing the number of atoms in the model, while still missing the rest of the protein environment, or with long-range electrostatic effects due to the discrete point charge representation of the MM region, which are not recovered by the continuum solvation model. Given the local nature of the spectroscopic parameters considered here, it is unlikely that the latter is the leading cause for the rough convergence of the QM-only models. Indeed, for the QM/MM models, the difference between the effective ground state and first excited state is not affected by the absence of point charges starting from model $\mathbf{C}_{QM/MM}$ onward (see Figure 4).

Therefore, a point charge representation of the protein is sufficient to describe at least the directionality of the interactions (e.g., hydrogen bonds). However, these long-range electrostatic interactions do not appear to be the decisive factor for the investigated spectroscopic properties. Rather, we attribute the results to subtle structural restrictions imposed by the protein environment that are easily lost in the case of a QM-only treatment. In contrast to backbone constraints, which do preserve the main aspects of the secondary structure of the protein,[29] the types of artifacts described previously are more difficult to remove in a QM-only description without costly enlargement of the model until the region from which the effect originates is explicitly included. Given the size and structural complexity of the present systems, it is also possible that some of the differences between QM and QM/MM results may reflect convergence to different conformers during geometry optimization.

In this respect, it is interesting to examine whether the convergence in each approach is monotonic or not: Figure 5 shows the average root-mean-square (RMS) displacement of

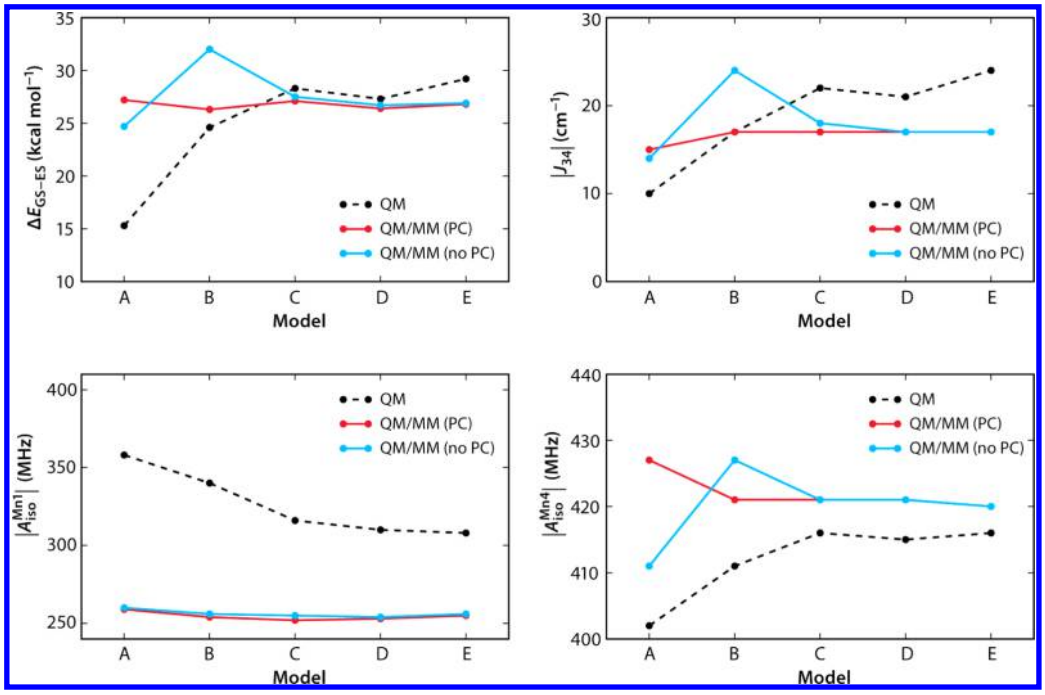

Figure 4. Convergence of properties with increasing model size for QM-only and QM/MM models with and without point charges (PC). Top: energetic separation between the ground state and first excited state energy (left) and J_{34} exchange coupling constant (right). Bottom: raw isotropic hyperfine coupling constant of Mn1 (left) and Mn4 (right).

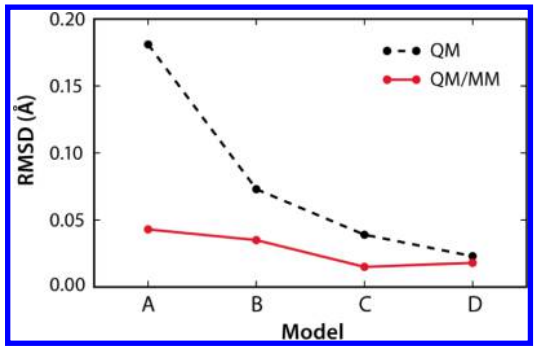

Figure 5. Average RMS displacement of the metal ions of the Mn_4CaO_5 core of models **A**–**D** with respect to the structure of model **E**: comparison of QM and QM/MM convergence.

the Mn and Ca ions of the OEC for each successively larger model, compared to the largest models, $\mathbf{E}_{QM/MM}$ and $\mathbf{E}_{QM}$, for the QM/MM and QM approaches, respectively. Although the same RMSD is achieved at model **D** for both methods, the smaller QM models display considerably higher deviations compared with the QM/MM models that have the same size QM region, to the point where the results obtained from model $\mathbf{A}_{QM}$ can even be considered misleading. An important observation is that there are no fluctuations in RMSDs; therefore the core does not tend to converge toward different conformers at successive enlargement steps. This does not have to be considered a result of general validity, as it probably depends on both the starting geometry at each step and on the choice of residues to include at each enlargement step; as described above, we opted for a chemically sensible enlargement protocol rather than a "blind" distance-based one. A second important observation is that the smaller QM-only models display large deviations in the core despite the presence of backbone constraints. In other words, freezing the alpha carbons of the protein backbone and thus restraining the overall spatial extent of the model does not guarantee convergence in bonded parameters even at the core of the model, because critical environmental effects are still missing.

The situation for the ligand hyperfine coupling constants is somewhat different. Whereas the calculated values for the ^{14}N HFC are similar for all QM-only models, and in perfect agreement with the values obtained with QM/MM, no clear trend, but also a large spread, was observed for the ^{17}O HFCs (Table 5). These react with extreme sensitivity to the size of the

Table 5. Calculated Values for the Unscaled and Unprojected ^{17}O and ^{14}N Isotropic Hyperfine Coupling Constants (MHz) of QM-only Models

	O5	W1	W2	Nε (His332)
$\mathbf{A}_{QM}$	−34.5	−10.8	−1.3	−12.4
$\mathbf{B}_{QM}$	−8.3	−22.8	−6.2	−12.8
$\mathbf{C}_{QM}$	−1.9	−11.6	−4.8	−12.7
$\mathbf{D}_{QM}$	−2.9	−11.4	−5.2	−12.4
$\mathbf{E}_{QM}$	−8.1	−4.6	0.5	−12.8

QM model, an effect most pronounced for the ^{17}O hyperfine coupling constant of water W1. For example, the inclusion of Asp61, which is not present in model $\mathbf{A}_{QM}$, leads to the deprotonation of W1, which in turn explains the dramatic increase in the calculate HFC value. With the addition of the extra water molecules in model $\mathbf{C}_{QM}$—HOH442 and HOH539 interact directly with Asp61—the calculated value is again strongly perturbed. However, it is only with the largest QM-only model, $\mathbf{E}_{QM}$, which includes the nearby D2-Lys317 that interacts with water HOH539, that good agreement with the QM/MM models can be obtained. Overall, the comparison between the QM/MM and QM-only results for the ^{17}O HFCs shows that the QM-only models are susceptible to large fluctuations of local electrostatic interactions and hydrogen-bonding patterns, or alternatively of protonation constants, leading to similarly large fluctuations in the predicted spectroscopic properties. Convergence with the QM models can of course be achieved (note however that in the present case even the largest model $\mathbf{E}_{QM}$ may be considered insufficiently converged for the ^{17}O HFCs), but apparently at considerably higher cost than with the QM/MM models.

3.5. Second-Sphere Effects. There are three charged amino acid residues in the second coordination sphere of the OEC, two provided by the D1 protein (Asp61 and His337) and one by the CP43 protein (Arg357). We note that second-sphere residues are as strongly preserved across aerobic photosynthetic organisms as the first-sphere ones.[90] Asp61 hydrogen-bonds directly to one of the two water ligands of Mn4 and hence appears to be the most closely involved in the chemistry of the catalyst. The importance of this negatively charged residue is highlighted by its position at the point of convergence of two apparent pathways: a proton-exit pathway that involves the proximal chloride ion and a water channel that is presumably used for substrate delivery.[91,92] Additionally, it is an important determinant of substrate water exchange kinetics.[93] CP43-Arg357 interacts with the OEC via multiple hydrogen bonding that dictates a preferred orientation for the guanidinium plane. Even though the precise structural or functional role of this residue has not been clarified yet, it is of interest to note that McEvoy and Brudvig have proposed that CP43-Arg357 may be involved in proton removal during the S_2–S_3 and S_3–$[S_4]$–S_0 transitions of the OEC. The third amino acid residue under consideration, His337, appears to be the persistent hydrogen bonding partner of O3 and may be the only side chain of the protein that directly interacts with an oxo bridge of the Mn_4CaO_5 core. In the following, the individual and combined effects that the presence or absence of these residues have on the properties of the OEC are determined and discussed in detail.

In model **A**, as well as in the other models, His337 is doubly protonated. In the optimized structure and in the crystal structure, τ-N (Nε) is hydrogen bonded to the O3 of the OEC core, while π-N (Nδ) is involved in a hydrogen bond with HOH381 (in the numbering followed in the crystal structure). In Table 6, we note a good correlation between the deletion of the atomic point charges of this residue and the concomitant perturbations on the exchange pathways mediated by O3. By

Table 6. Calculated Exchange Coupling Constants of Model A with Different Sets of Deleted Atomic Point Charges

	J_{12}	J_{13}	J_{14}	J_{23}	J_{24}	J_{34}	ΔE_{ES-GS}
none	−20	1	5	19	2	−15	27.2
CP43-Arg357	−19	1	4	29	2	−15	26.1
Asp61	−19	0	8	20	2	−13	24.1
His337	−25	4	5	15	3	−15	27.2
Arg357, Asp61, His337	−23	3	8	24	3	−13	23.9
all	−23	4	7	23	3	−14	24.7

dx.doi.org/10.1021/ct400477j | J. Chem. Theory Comput. 2013, 9, 3832–3842

contrast, the effect on the other exchange interactions is negligible, with no change at all for J_{34}. Similar trends are observed for CP43-Arg357 and Asp61. A marked influence can be noted in the exchange coupling constants if their hydrogen bonding partners mediate—J_{23} in the case of CP43-Arg357—or are adjacent—J_{14} in the case of Asp61—to the centers involved in the interaction. Also reported in Table 6 are the results obtained by simultaneous deletion of the charges on all three amino acids—His337, CP41-Arg357, and Asp61. The calculated exchange coupling constants are comparable to the values obtained from a gas phase calculation, i.e. without point charges.

Overall, the results obtained by "switching off"—in turn or together—the aforementioned residues suggest a significant influence of the second coordination sphere on the magnetic properties of the inorganic core and a limited effect of the remaining protein environment. This parallels the results obtained with increasingly large QM region, where the exchange coupling constants obtained with model **B** can be considered converged.

3.6. Rotational Effects of His332 on the Mn1 Hyperfine Coupling Constant. His332 has a "special status" in the OEC for at least two reasons: (a) it is the only N-donor ligand present, and (b) it is coordinated to the unique Mn(III) ion of the S_2 state. As such, it has been employed as a probe for the electronic structure of Mn1, since the ^{14}N hyperfine coupling constant of the coordinating atom is diagnostic of the oxidation state of the metal ion.

In the first part of this work, we pointed out that rotation of the imidazole ring of His332 is expected to be inhibited because of the hydrogen bond between the protonated π-N (Nδ) of the imidazole and the carbonyl group of the Glu329 peptide bond (Figure 6). This hydrogen bond is present in all QM/MM

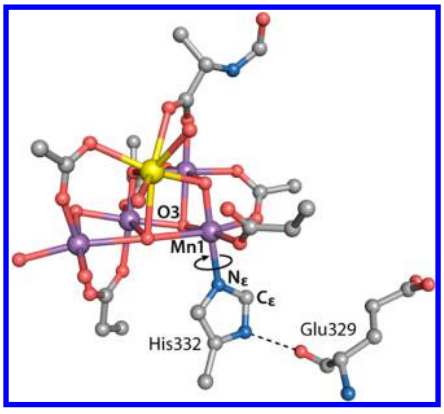

Figure 6. Model **A** and Glu329, showing the hydrogen bonding interaction with the Nδ of His332. The O3−Mn1−Nε−Cε dihedral angle that determines the orientation of His332 with respect to the Mn_4CaO_5 core is indicated.

models reported here and—judging from the short N···O distance of 2.65 Å and the N···O C angle of 127°—in the crystal structure as well. We have also hypothesized that this rotation, which for the QM-only model of **A** leads to a quasi-alignment of the imidazole ring of His332 with the Mn1−O3 bond, was one of the factors responsible for the significant increase of the isotropic HFC coupling constant of Mn1.

Here, we examine the implications of this rotational restriction for the magnetic properties of the Mn1 ion, by means of a relaxed scan of the O3−Mn1−Nε−Cε dihedral angle using the QM-only representation of model **A**. In order to separate the rotational effect from other structural differences that may affect the calculated parameters, only the positions of the atoms from the imidazole ring and the hydrogens bound to the Cα atom were allowed to relax (the corresponding energy barrier for rotation is approximately 4 kcal mol^{-1}). We will again limit ourselves to discussing the raw—unscaled and unprojected—hyperfine coupling constants of Mn1.

The calculated A_{iso} using the 21 structures along the scan path are plotted in Figure 7. There is a difference of

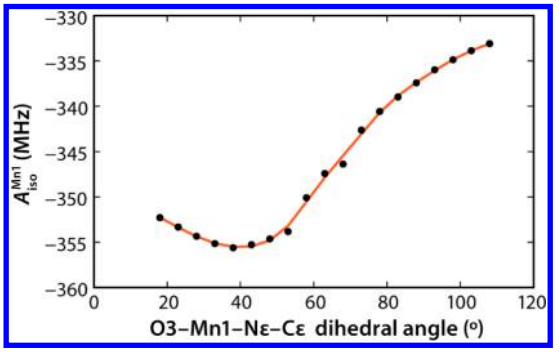

Figure 7. Dependence of the Mn1 isotropic hyperfine coupling constant on the rotation of the His332 imidazole ring.

approximately 25 MHz between values corresponding to the dihedral angle in the optimized QM/MM (103°) and the QM-only (36°) models of **A**. Thus, part of the previously observed 100 MHz difference in absolute value of A_{iso} can be assigned to the rotation of the imidazole ring of His332. Nevertheless, it is reasonable to presume that the rotation will also affect other nearby residues, resulting in structural changes of the coordination environment of the Mn1 ion.

4. CONCLUSIONS

Questions related to the sensitivity of calculated properties with respect to the size of the QM region in QM-only and QM/MM approaches have been addressed by many groups, with most of the studies focusing mainly on reaction energetics,[94−99] although spectroscopic properties have also been considered for certain systems.[100−106] Answers to such questions are unavoidably dependent on the nature of the specific chemical system and the properties under investigation; the two methods can be most fruitfully viewed as complementary. Of course, in the limit of large QM regions the two approaches should in principle provide similar or equivalent results; in practice, the limit can often be attained faster by the QM/MM approach. This is indeed the case also in the present work for the spectroscopic properties of the OEC.

The structural parameters, the magnetic interactions expressed as exchange coupling constants between the manganese ions, and the hyperfine coupling constants of the metal and the ligand atoms converge quite fast with the QM/MM models. Among the five QM regions considered in this study, ranging from 92 to 225 QM atoms, the second largest model with 131 atoms already yields results that are sufficiently converged for most properties. Incorporation in the QM region of all second-sphere residues (Asp61, His337, and CP43-Arg357), which hydrogen-bond to the Mn_4CaO_5 cluster or to first-sphere ligands, is still necessary in the QM/MM treatment. The gains achieved by increasing the QM region even further are rather limited for the properties examined in this work. QM-only

treatments require at least one additional enlargement step with vicinal water molecules to ensure proper hydrogen bonding and thus to show initial convergence for structural and magnetic properties. However, even with fairly large QM-only cluster models of the OEC and the imposition of backbone constraints, the absence of certain structural and electronic effects arising from directional electrostatic interactions and hydrogen bonds that originate beyond the explicitly treated QM-only model may still lead to artifacts that delay convergence for specific properties. This is found here both for the ^{17}O hyperfine coupling constants of Mn-bound waters and for the rotation of His332, which is shown to influence the spectroscopic signature of the Mn(III) center. These problems can be removed in the QM-only treatment by continuous enlargement of the cluster model; however a carefully calibrated QM/MM approach seems able to achieve converged results at a reduced cost.

■ ASSOCIATED CONTENT

Supporting Information

Tables S1−S4 and Cartesian coordinates of the QM regions for all optimized structures. This material is available free of charge via the Internet at http://pubs.acs.org.

■ AUTHOR INFORMATION

Corresponding Author

*E-mail: dimitrios.pantazis@cec.mpg.de.

Notes

The authors declare no competing financial interest.

■ ACKNOWLEDGMENTS

Financial support was provided by the Max Planck Society.

■ REFERENCES

(1) Blankenship, R. E. *Molecular Mechanisms of Photosynthesis*; Blackwell: Oxford, 2001; p 321.

(2) *Photosystem II. The Light-Driven Water:Plastoquinone Oxidoreductase*; Wydrzynski, T., Satoh, K., Eds.; Springer: Dordrecht, The Netherlands, 2005; Vol. *22*

(3) Messinger, J.; Alia, A.; Govindjee *Photosynth. Res.* **2009**, *101/102*, 89−266; 103−347; Special Issues: Basics and Applications of Biophysical Techniques in Photosynthesis and Related Processes - Parts A and B .

(4) Messinger, J.; Renger, G. In *Primary Processes of Photosynthesis, Part 2: Principles and Apparatus*; The Royal Society of Chemistry: Cambridge, U. K., 2008; Vol. *9*, pp 291−349.

(5) McEvoy, J. P.; Brudvig, G. W. *Chem. Rev.* **2006**, *106*, 4455−4483.

(6) Cox, N.; Lubitz, W. In *Chemical Energy Storage*; Schlögl, R., Ed.; De Gruyter: Berlin, 2013; pp 185−224.

(7) Cox, N.; Pantazis, D. A.; Neese, F.; Lubitz, W. *Acc. Chem. Res.* **2013**, *46*, 1588−1596.

(8) Neese, F.; Ames, W.; Christian, G.; Kampa, M.; Liakos, D. G.; Pantazis, D. A.; Roemelt, M.; Surawatanawong, P.; Ye, S. F. *Adv. Inorg. Chem.* **2010**, *62*, 301−349.

(9) Neese, F. *Coord. Chem. Rev.* **2009**, *253*, 526−563.

(10) Lubitz, W.; Reijerse, E. J.; Messinger, J. *Energy Environ. Sci* **2008**, *1*, 15−31.

(11) DeBeer, S.; van Gastel, M.; Bill, E.; Ye, S.; Petrenko, T.; Pantazis, D. A.; Neese, F. In *Chemical Energy Storage*; Schlögl, R., Ed.; De Gruyter: Berlin, 2013, p 353−377.

(12) Dau, H.; Zaharieva, I. *Acc. Chem. Res.* **2009**, *42*, 1861−1870.

(13) Lin, H.; Truhlar, D. G. *Theor. Chem. Acc.* **2007**, *117*, 185−199.

(14) Senn, H. M.; Thiel, W. *Angew. Chem., Int. Ed.* **2009**, *48*, 1198−1229.

(15) Umena, Y.; Kawakami, K.; Shen, J.-R.; Kamiya, N. *Nature* **2011**, *473*, 55−60.

(16) Ferreira, K. N.; Iverson, T. M.; Maghlaoui, K.; Barber, J.; Iwata, S. *Science* **2004**, *303*, 1831−1838.

(17) Sproviero, E. M.; Gascon, J. A.; McEvoy, J. P.; Brudvig, G. W.; Batista, V. S. *J. Chem. Theory Comput.* **2006**, *2*, 1119−1134.

(18) Sproviero, E. M.; Gascon, J. A.; McEvoy, J. P.; Brudvig, G. W.; Batista, V. S. *Curr. Opin. Struct. Biol.* **2007**, *17*, 173−180.

(19) Sproviero, E. M.; Gascon, J. A.; McEvoy, J. P.; Brudvig, G. W.; Batista, V. S. *J. Am. Chem. Soc.* **2008**, *130*, 6728−6730.

(20) Sproviero, E. M.; Gascon, J. A.; McEvoy, J. P.; Brudvig, G. W.; Batista, V. S. *J. Am. Chem. Soc.* **2008**, *130*, 3428−3442.

(21) Sproviero, E. M.; Shinopoulos, K.; Gascon, J. A.; McEvoy, J. P.; Brudvig, G. W.; Batista, V. S. *Philos. Trans. R. Soc. London, Ser. B* **2008**, *363*, 1149−1156.

(22) Sproviero, E. M.; Gascon, J. A.; McEvoy, J. P.; Brudvig, G. W.; Batista, V. S. *Coord. Chem. Rev.* **2008**, *252*, 395−415.

(23) Sproviero, E.; Newcomer, M.; Gascón, J.; Batista, E.; Brudvig, G.; Batista, V. *Photosynth. Res.* **2009**, *102*, 455−470.

(24) Siegbahn, P. E. M. *J. Am. Chem. Soc.* **2009**, *131*, 18238−18239.

(25) Guskov, A.; Kern, J.; Gabdulkhakov, A.; Broser, M.; Zouni, A.; Saenger, W. *Nat. Struct. Mol. Biol.* **2009**, *16*, 334−342.

(26) Kawakami, K.; Umena, Y.; Kamiya, N.; Shen, J.-R. *Proc. Natl. Acad. Sci. U.S.A.* **2009**, *106*, 8567−8572.

(27) Luber, S.; Rivalta, I.; Umena, Y.; Kawakami, K.; Shen, J. R.; Kamiya, N.; Brudvig, G. W.; Batista, V. S. *Biochemistry* **2011**, *50*, 6308−6311.

(28) Siegbahn, P. E. M. *Chem.—Eur. J.* **2008**, *14*, 8290−8302.

(29) Siegbahn, P. E. M. *ChemPhysChem* **2011**, *12*, 3274−3280.

(30) Siegbahn, P. E. M. *Inorg. Chem.* **2008**, *47*, 1779−1786.

(31) Siegbahn, P. E. M. *Philos. Trans. R. Soc. London, Ser. B* **2008**, *363*, 1221−1228.

(32) Siegbahn, P. E. M. *Acc. Chem. Res.* **2009**, *42*, 1871−1880.

(33) Siegbahn, P. E. M. *J. Photochem. Photobiol., B* **2011**, *104*, 94−99.

(34) Pantazis, D. A.; Orio, M.; Petrenko, T.; Zein, S.; Lubitz, W.; Messinger, J.; Neese, F. *Phys. Chem. Chem. Phys.* **2009**, *11*, 6788−6798.

(35) Cox, N.; Rapatskiy, L.; Su, J.-H.; Pantazis, D. A.; Sugiura, M.; Kulik, L.; Dorlet, P.; Rutherford, A. W.; Neese, F.; Boussac, A.; Lubitz, W.; Messinger, J. *J. Am. Chem. Soc.* **2011**, *133*, 3635−3648.

(36) Su, J.-H.; Cox, N.; Ames, W.; Pantazis, D. A.; Rapatskiy, L.; Lohmiller, T.; Kulik, L. V.; Dorlet, P.; Rutherford, A. W.; Neese, F.; Boussac, A.; Lubitz, W.; Messinger, J. *Biochim. Biophys. Acta Bioenerg.* **2011**, *1807*, 829−840.

(37) Ames, W.; Pantazis, D. A.; Krewald, V.; Cox, N.; Messinger, J.; Lubitz, W.; Neese, F. *J. Am. Chem. Soc.* **2011**, *133*, 19743−19757.

(38) Pantazis, D. A.; Ames, W.; Cox, N.; Lubitz, W.; Neese, F. *Angew. Chem., Int. Ed.* **2012**, *51*, 9935−9940.

(39) Pantazis, D. A.; Orio, M.; Petrenko, T.; Zein, S.; Bill, E.; Lubitz, W.; Messinger, J.; Neese, F. *Chem.—Eur. J.* **2009**, *15*, 5108−5123.

(40) Isobe, H.; Shoji, M.; Koizumi, K.; Kitagawa, Y.; Yamanaka, S.; Kuramitsu, S.; Yamaguchi, K. *Polyhedron* **2005**, *24*, 2767−2777.

(41) Yamaguchi, K.; Yamanaka, S.; Isobe, H.; Shoji, M.; Koizumi, K.; Kitagawa, Y.; Kawakami, T.; Okumura, M. *Polyhedron* **2007**, *26*, 2216−2224.

(42) Kanda, K.; Yamanaka, S.; Saito, T.; Umena, Y.; Kawakami, K.; Shen, J.-R.; Kamiya, N.; Okumura, M.; Nakamura, H.; Yamaguchi, K. *Chem. Phys. Lett.* **2011**, *506*, 98−103.

(43) Yamanaka, S.; Isobe, H.; Kanda, K.; Saito, T.; Umena, Y.; Kawakami, K.; Shen, J. R.; Kamiya, N.; Okumura, M.; Nakamura, H.; Yamaguchi, K. *Chem. Phys. Lett.* **2011**, *511*, 138−145.

(44) Isobe, H.; Shoji, M.; Yamanaka, S.; Umena, Y.; Kawakami, K.; Kamiya, N.; Shen, J. R.; Yamaguchi, K. *Dalton Trans.* **2012**, *41*, 13727−13740.

(45) Saito, T.; Shoji, M.; Kanda, K.; Isobe, H.; Yamanaka, S.; Kitagawa, Y.; Yamada, S.; Kawakami, T.; Okumura, M.; Yamaguchi, K. *Int. J. Quantum Chem.* **2012**, *112*, 121−135.

(46) Saito, T.; Yamanaka, S.; Kanda, K.; Isobe, H.; Takano, Y.; Shigeta, Y.; Umena, Y.; Kawakami, K.; Shen, J. R.; Kamiya, N.;

Okumura, M.; Shoji, M.; Yoshioka, Y.; Yamaguchi, K. *Int. J. Quantum Chem.* **2012**, *112*, 253−276.
(47) Yamaguchi, K.; Isobe, H.; Yamanaka, S.; Saito, T.; Kanda, K.; Shoji, M.; Umena, Y.; Kawakami, K.; Shen, J. R.; Kamiya, N.; Okumura, M. *Int. J. Quantum Chem.* **2012**, *113*, 525−541.
(48) Yamaguchi, K.; Yamanaka, S.; Isobe, H.; Saito, T.; Kanda, K.; Umena, Y.; Kawakami, K.; Shen, J. R.; Kamiya, N.; Okumura, M.; Nakamura, H.; Shoji, M.; Yoshioka, Y. *Int. J. Quantum Chem.* **2013**, *113*, 453−473.
(49) Yamanaka, S.; Kanda, K.; Saito, T.; Umena, Y.; Kawakami, K.; Shen, J. R.; Kamiya, N.; Okumura, M.; Nakamura, H.; Yamaguchi, K. In *Adv. Quantum Chem.*; John, R. S., Erkki, J. B., Eds.; Academic Press: New York, 2012; Vol. *64*, pp 121−187.
(50) Yamanaka, S.; Saito, T.; Kanda, K.; Isobe, H.; Umena, Y.; Kawakami, K.; Shen, J. R.; Kamiya, N.; Okumura, M.; Nakamura, H.; Yamaguchi, K. *Int. J. Quantum Chem.* **2012**, *112*, 321−343.
(51) Kusunoki, M. *Photochem. Photobiol., B* **2011**, *104*, 100−110.
(52) Petrie, S.; Stranger, R.; Gatt, P.; Pace, R. J. *Chem.—Eur. J.* **2007**, *13*, 5082−5089.
(53) Petrie, S.; Stranger, R.; Pace, R. L. *Chem.—Eur. J.* **2008**, *14*, 5482−5494.
(54) Petrie, S.; Stranger, R.; Pace, R. J. *Angew. Chem., Int. Ed.* **2010**, *49*, 4233−4236.
(55) Petrie, S.; Stranger, R.; Pace, R. J. *Chem.—Eur. J.* **2010**, *16*, 14026−14042.
(56) Jaszewski, A. R.; Petrie, S.; Pace, R. J.; Stranger, R. *Chem.—Eur. J.* **2011**, *17*, 5699−5713.
(57) Gatt, P.; Petrie, S.; Stranger, R.; Pace, R. J. *Angew. Chem., Int. Ed.* **2012**, *51*, 12025−12028.
(58) Pace, R. J.; Jin, L.; Stranger, R. *Dalton Trans.* **2012**, *41*, 11145−11160.
(59) Petrie, S.; Gatt, P.; Stranger, R.; Pace, R. J. *Phys. Chem. Chem. Phys.* **2012**, *14*, 4651−4657.
(60) Petrie, S.; Gatt, P.; Stranger, R.; Pace, R. J. *Phys. Chem. Chem. Phys.* **2012**, *14*, 11333−11343.
(61) Schinzel, S.; Schraut, J.; Arbuznikov, A. V.; Siegbahn, P. E. M.; Kaupp, M. *Chem.—Eur. J.* **2010**, *16*, 10424−10438.
(62) Ichino, T.; Yoshioka, Y. *Bull. Chem. Soc. Jpn.* **2013**, *86*, 479−491.
(63) Rapatskiy, L.; Cox, N.; Savitsky, A.; Ames, W. M.; Sander, J.; Nowaczyk, M. M.; Rögner, M.; Boussac, A.; Neese, F.; Messinger, J.; Lubitz, W. *J. Am. Chem. Soc.* **2012**, *134*, 16619−16634.
(64) Orio, M.; Pantazis, D. A.; Petrenko, T.; Neese, F. *Inorg. Chem.* **2009**, *48*, 7251−7260.
(65) Jorgensen, W. L.; Maxwell, D. S.; Tirado-Rives, J. *J. Am. Chem. Soc.* **1996**, *118*, 11225−11236.
(66) Jorgensen, W. L.; Chandrasekhar, J.; Madura, J. D.; Impey, R. W.; Klein, M. L. *J. Chem. Phys.* **1983**, *79*, 926−935.
(67) Olsson, M. H. M.; Søndergaard, C. R.; Rostkowski, M.; Jensen, J. H. *J. Chem. Theory Comput.* **2011**, *7*, 525−537.
(68) Pronk, S.; Páll, S.; Schulz, R.; Larsson, P.; Bjelkmar, P.; Apostolov, R.; Shirts, M. R.; Smith, J. C.; Kasson, P. M.; van der Spoel, D.; Hess, B.; Lindahl, E. *Bioinformatics* **2013**, *29*, 845−854.
(69) Perdew, J. P. *Phys. Rev. B* **1986**, *33*, 8822−8824.
(70) Becke, A. D. *Phys. Rev. A* **1988**, *38*, 3098−3100.
(71) van Lenthe, E.; Baerends, E. J.; Snijders, J. G. *J. Chem. Phys.* **1993**, *99*, 4597−4610.
(72) van Lenthe, E.; Baerends, E. J.; Snijders, J. G. *J. Chem. Phys.* **1994**, *101*, 9783−9792.
(73) van Lenthe, E.; Snijders, J. G.; Baerends, E. J. *J. Chem. Phys.* **1996**, *105*, 6505−6516.
(74) van Wüllen, C. *J. Chem. Phys.* **1998**, *109*, 392−399.
(75) Pantazis, D. A.; Chen, X. Y.; Landis, C. R.; Neese, F. *J. Chem. Theory Comput.* **2008**, *4*, 908−919.
(76) Weigend, F.; Ahlrichs, R. *Phys. Chem. Chem. Phys.* **2005**, *7*, 3297−3305.
(77) Weigend, F. *Phys. Chem. Chem. Phys.* **2006**, *8*, 1057−1065.
(78) Grimme, S.; Antony, J.; Ehrlich, S.; Krieg, H. *J. Chem. Phys.* **2010**, *132*, 154104−19.
(79) Lin, H.; Truhlar, D. G. *J. Phys. Chem. A* **2005**, *109*, 3991−4004.
(80) Field, M. J. *J. Chem. Theory Comput.* **2008**, *4*, 1151−1161.
(81) Neese, F. *WIREs Comput. Mol. Sci.* **2012**, *2*, 73−78.
(82) Klamt, A.; Schüürman, D. *J. Chem. Soc., Perkin Trans. 2* **1993**, 799−805.
(83) Baffert, C.; Orio, M.; Pantazis, D. A.; Duboc, C.; Blackman, A. G.; Blondin, G.; Neese, F.; Deronzier, A.; Collomb, M.-N. *Inorg. Chem.* **2009**, *48*, 10281−10288.
(84) Orio, M.; Pantazis, D. A.; Neese, F. *Photosynth. Res.* **2009**, *102*, 443−453.
(85) Pantazis, D. A.; Krewald, V.; Orio, M.; Neese, F. *Dalton Trans.* **2010**, *39*, 4959−4967.
(86) Krewald, V.; Neese, F.; Pantazis, D. A. *J. Am. Chem. Soc.* **2013**, *135*, 5726−5739.
(87) Staroverov, V. N.; Scuseria, G. E.; Tao, J.; Perdew, J. P. *J. Chem. Phys.* **2003**, *119*, 12129−12137.
(88) Yano, J.; Pushkar, Y.; Glatzel, P.; Lewis, A.; Sauer, K.; Messinger, J.; Bergmann, U.; Yachandra, V. *J. Am. Chem. Soc.* **2005**, *127*, 14974−14975.
(89) Pushkar, Y.; Yano, J.; Sauer, K.; Boussac, A.; Yachandra, V. K. *Proc. Natl. Acad. Sci. U. S. A.* **2008**, *105*, 1879−1884.
(90) Renger, G.; Ludwig, B. In *Bioenergetic Processes of Cyanobacteria - from Evolutionary Singularity to Ecological Diversity*; Peschek, G., Obinger, C., Renger, G., Eds.; Springer: Dordrecht, The Netherlands, 2011; pp 337−394.
(91) Vassiliev, S.; Zaraiskaya, T.; Bruce, D. *Biochim. Biophys. Acta Bioenerg* **2012**, *1817*, 1671−1678.
(92) Rivalta, I.; Amin, M.; Luber, S.; Vassiliev, S.; Pokhrel, R.; Umena, Y.; Kawakami, K.; Shen, J. R.; Kamiya, N.; Bruce, D.; Brudvig, G. W.; Gunner, M. R.; Batista, V. S. *Biochemistry* **2011**, *50*, 6312−6315.
(93) Singh, S.; Debus, R. J.; Wydrzynski, T.; Hillier, W. *Phil. Trans. R. Soc. London, Ser. B* **2008**, *363*, 1229−1235.
(94) Sumowski, C. V.; Ochsenfeld, C. *J. Phys. Chem. A* **2009**, *113*, 11734−11741.
(95) Stanton, C. L.; Kuo, I. F. W.; Mundy, C. J.; Laino, T.; Houk, K. N. *J. Phys. Chem. B* **2007**, *111*, 12573−12581.
(96) van der Kamp, M. W.; Żurek, J.; Manby, F. R.; Harvey, J. N.; Mulholland, A. J. *J. Phys. Chem. B* **2010**, *114*, 11303−11314.
(97) Siegbahn, P. E. M.; Himo, F. *WIREs Comput. Mol. Sci.* **2011**, *1*, 323−336.
(98) Liao, R.-Z.; Thiel, W. *J. Chem. Theory Comput.* **2012**, *8*, 3793−3803.
(99) Hu, L.; Söderhjelm, P.; Ryde, U. *J. Chem. Theory Comput.* **2013**, *9*, 640−649.
(100) Waller, M. P.; Geethalakshmi, K. R.; Bühl, M. *J. Phys. Chem. B* **2008**, *112*, 5813−5823.
(101) Geethalakshmi, K. R.; Waller, M. P.; Thiel, W.; Bühl, M. *J. Phys. Chem. B* **2009**, *113*, 4456−4465.
(102) Baer, M.; Mathias, G.; Kuo, I. F. W.; Tobias, D. J.; Mundy, C. J.; Marx, D. *ChemPhysChem* **2008**, *9*, 2703−2707.
(103) López-Canut, V.; Martí, S.; Bertrán, J.; Moliner, V.; Tuñón, I. *J. Phys. Chem. B* **2009**, *113*, 7816−7824.
(104) Hirao, H.; Morokuma, K. *J. Phys. Chem. Lett.* **2010**, *1*, 901−906.
(105) Rinkevicius, Z.; Murugan, N. A.; Kongsted, J.; Frecuş, B.; Steindal, A. H.; Ågren, H. *J. Chem. Theory Comput.* **2011**, *7*, 3261−3271.
(106) Flaig, D.; Beer, M.; Ochsenfeld, C. *J. Chem. Theory Comput.* **2012**, *8*, 2260−2271.